OEDGE modeling of ^{13}C Deposition in the Inner Divertor of DIII-D

J.D. Elder[a], P.C. Stangeby[a,b,c], D. G. Whyte[d], S. Allen[c], A. McLean[ab], J. Boedo[e], B.D. Bray[b], N.H. Brooks[b], M.E. Fenstermacher[c], M. Groth[c], C. Lasnier[c], S. Lisgo[a], D.L. Rudakov[e], W.R. Wampler[f], J.G. Watkins[f], W.P. West[b]

[a]*University of Toronto Institute for Aerospace Studies*

[b]*General Atomics*

[c]*Lawrence Livermore National Laboratory*

[d]*University of Wisconsin – Madison*

[e]*Univeristy of California – San Diego*

[f]*Sandia National Laboratory.*

Abstract

Carbon leads to a major tritium retention issue due to co-deposition. To test the transport and deposition aspects of this process a SAPP (simple as possible plasma) L-mode experiment was performed on DIII-D in which $^{13}CH_4$ was puffed into the main vessel through the toroidally-symmetric pumping plenum at the top of LSN discharges[1]. Subsequently, the ^{13}C content of tiles taken from the vessel wall was measured[2]. This paper is on modeling the transport and deposition using the interpretive OEDGE code. It was found that the ^{13}C deposition pattern is controlled by: (a) source strength of $^{13}C^+$, (b) radial location of the $^{13}C^+$ source, (c) $D_\perp$, (d) $M_\parallel$, the SOL parallel Mach number. Best agreement was found for (a) ~50% conversion efficiency $^{13}CH_4 \rightarrow {}^{13}C^+$, (b) $^{13}C^+$ source ~ 3.5 cm outboard of separatrix near $^{13}CH_4$ injection location, (c) $D_\perp \sim 0.3$ m^2s^{-1}, (d) $M_\parallel \sim 0.4$ toward inside.

JNM keywords: T0100, C0100 I0100, P0600, D0500

PSI-16 keywords: Carbon Impurities, DIII-D, Edge Modeling, Impurity Transport, OEDGE

PACS: 52.65 Plasma Simulation

[*]*Corresponding author address:*

David Elder

University of Toronto Institute for Aerospace Studies

4925 Dufferin St., Downsview

ON. CANADA

M3H 5T6

**Corresponding author e-mail:*

david@starfire.utias.utoronto.ca

Presenting author address: ***See above***

Presenting author e-mail: ***See above***

Introduction

Carbon is a candidate plasma facing material in many fusion reactor designs. It has many advantageous properties including ease of machining, low atomic number – and it does not melt. Unfortunately, when carbon deposits on a surface, hydrogenic plasma particles also deposit. This co-deposition process does not saturate and could result in an unacceptable build up of tritium inventory in co-deposited layers on vessel surfaces. There are three principal questions: (1) What is the source of the carbon? (2) What transport mechanism carries the carbon to the inner target? (3) What factors determine the final resting place of the carbon and the build up of co-deposited layers in the inner divertor? This paper is an interpretive modeling investigation related to the 2nd and 3rd questions.

A well-controlled low power, ~ 1 MW, SAPP (simple as possible plasma) L-mode experiment was run on DIII-D in which ^{13}C methane was puffed through the upper pumping plenum of LSN discharges[1]. This puff was toroidally symmetric and at a rate which did not significantly perturb the local plasma conditions. The puff rate was limited so that the increase in the measured carbon density in the core was modest, ~ 25%. The ^{13}C was puffed for 22 consecutive identical discharges for a period of 3 seconds during each discharge under steady state plasma conditions. After the experiment, 29 tiles were removed and the ^{13}C content was measured using nuclear reaction analysis[2]. Detectable ^{13}C deposition was only found for tiles in the inner divertor region.

The OEDGE (Osm Eirene Divimp edGE) code[4] was used in this study to model the transport and deposition of the ^{13}C. The objective was to identify and quantify the controlling factors governing the ^{13}C deposition pattern. It is found that the ^{13}C deposition pattern and core ^{13}C-content are essentially controlled by 4 quantities: (a) the source strength of $^{13}C^{+}$, (b) the radial

location of the $^{13}C^{+}$ source, (c) $D_{\perp}$, (d) $M_{||}$, the parallel Mach number. Large values of $M_{||}$ toward the inside, in the SOL at the top (LSN divertor), have been measured in a number of tokamaks, but attempts to explain/model this flow have been unsuccessful to date. Separately reported OEDGE analysis[3] is used to model (a) and (b). Here all 4 control parameters are treated as unknowns and the range of their permitted values is 'backed out' of the interpretive code analysis by comparison with the experimental measurements.

Results

The first step in the OEDGE analysis was to use all available experimental data and the 'onion-skin' modeling (OSM) in OEDGE to infer a solution for the background plasma by empirical reconstruction. (There insufficient space in the present paper to adequately describe this modeling method, but a very similar reconstruction exercise, also for a detached DIII-D divertor case, is reported in these proceedings[5]) This plasma solution (identified as OSM in the figures) is then used as the basis for calculating the transport and deposition of the ^{13}C in the rest of the study. The experimental data used here included calibrated spectroscopic measurements of D_{α}, D_{β} and D_{γ} for both the inner and outer targets, target Langmuir probe measurements of I_{sat}^{+}, calibrated spectroscopic data for various carbon emission lines, and upstream measurements of the plasma conditions by both Thomson and reciprocating probe. The plasma solution obtained by this empirical modeling used the Langmuir probe I_{sat}^{+} as input (Fig. 1) and matched the hydrogenic spectroscopy (Fig. 2) at the inner and outer targets as well as the upstream plasma measurements (Fig. 3). The inner target was found to be detached with a near target plasma temperature of $0.8 \pm \sim 0.2$ eV. The D_{α}, D_{β}, D_{γ} are extremely sensitive "T_e thermometers" in these cold, dense conditions, providing most valuable, and precise, input to the empirical reconstruction of the inner plasma, see Ref 5.

Superimposed by the code on the plasma solution was a parallel plasma flow of specified Mach number, $M_{||}$, extending from near the outer target to near the inner one.

The ^{13}C deposition measurements found no significant ^{13}C deposition (above background) anywhere other than the inner target region. The experimental deposition is shown with the model results below.

A series of simulations were run where the parallel flow was specified varying from $M_{||}$ = 0.05 up to $M_{||}$ = 2. In this set of simulations, ^{13}C was launched in DIVIMP as $^{13}C^{+}$ at a single radial upstream position, 3.5 cm outboard of the separatrix, near the top of the torus in the vicinity of the $^{13}CH_4$ puff. A constant value of $D_{\perp}$= 0.3m^2/s was also used . The calculated ^{13}C deposition patterns are shown in figure 4. The experimental profile is best matched by $M_{||}$ of ~ 0.4. If the flow in the SOL is too slow the deposition spreads out on the inner target and significant deposition is seen on the inner wall – contrary to observation. If the SOL flow is too fast then the deposition profile on the inner target becomes too narrow. This result indicates that the SOL flow lies in the range $M_{||}$ = ~ 0.3 - 0.6 directed toward the inside. Assumption of flow, at any speed, toward the outside completely fails to match the measured deposition pattern. For the code results shown in Fig 4 and the other comparisons below, a conversion efficiency of 50% was assumed. Raising/lowering the efficiency simply changes the vertical scale on these figures for the code results. It is thus evident that the efficiency is ~50% ± ~20%.

In the next study the parallel flow was fixed at $M_{||}$ = 0.4 across the SOL while the value of $D_{\perp}$ was varied. Singly charged ^{13}C ions were started at the same radial location as in the previous study. The deposition resulting from varying $D_{\perp}$ can be seen in figure 5. In this case, smaller

values of $D_\perp$ cause the target deposition profile to become more peaked while the larger $D_\perp$ values spread the deposition out across the target. The larger values of $D_\perp$ give more deposition on the inner wall. The transport is dominated by the parallel flow. It is concluded that $D_\perp \sim 0.3 - 0.5$.

In the next study, singly charged ^{13}C ions were started at different radial locations upstream. $M_\parallel = 0.4$ was specified as well as a $D_\perp$ value of $0.3 m^2/s$. The launch locations varied from inside the separatrix to the middle of the SOL. The deposition profiles for these different launch positions can be seen in figure 6. The radial locations in this figure are specified in terms of the perpendicular distance of the launch position from the separatrix. Clearly, the radial position of the initial ^{13}C significantly affects the target deposition pattern. Starting too far out in the SOL results in significant inner wall deposition and a target deposition peak located too far from the inner strike point. On the other hand, a source too close to the separatrix moves the deposition peak inward toward the strike point. It is concluded that the $^{13}C^+$ source is located at 3-6 cm outboard of the separatrix, at the poloidal location of the puff.

In addition to the deposition pattern, the total carbon density at the edge of the core places another constraint on the 4 control parameters. Table 1 shows the carbon core edge content for each of these simulations. The experimentally measured increment to the core carbon density just inside the separatrix as a result of the ^{13}C puff is 2.0e16 C/m^3, from charge exchange recombination spectroscopy (CER) measurements. It can be seen from this table that the simulations with $M_\parallel \sim 0.4$ to 0.6, $D_\perp \sim 0.3 m^2/s$, and ions starting at the 3.5cm flux surface are consistent with the total amount of carbon entering the core plasma as well as the deposition pattern.

For the majority of cases there is little or no deposition anywhere but in the inner divertor region. The only exception was for $M_{||} = -0.05$ where ~25% of the particles deposited on the inner wall and ~8% on the outer target.

Discussion

The foregoing analysis constitutes a first, simple treatment. It nevertheless appears adequate to identify approximate values for the 4 main control parameters. A number of refinements will be included in future work, including incorporation of computed C^+ source strength and its spatial distribution – both radially and poloidally. It is unlikely that $M_{||}$ is spatially constant, and when experimental information on its radial and poloidal variation is obtained, e.g. from detailed interpretive analysis of the CII, CIII 'cloud' shapes, this will also be incorporated. A potentially important effect, which has not been included in the present analysis, is the erosion and re-deposition of the ^{13}C particles which strike the inner target – i.e. the redistribution of the ^{13}C resulting from the ongoing plasma exposure. Preliminary modeling of the erosion and re-deposition patterns at the inner target indicates that the entire target is a net deposition region, which tends to justify the neglect of erosion and re-deposition *here*. This simplifying aspect of the present experiment cannot be expected generally: on JET, the ^{13}C that initially arrived at the inner target, did not stop there but continued on to deposit on adjacent surfaces that were out of plasma contact[6]. The rather low input power of the present L-mode SAPP experiment has resulted in this very valuable simplification. In future studies, erosion and re-deposition are likely to play a more important – and possibly totally dominating – role. Including this effect will constitute a substantially increased challenge to the modeling, since the details of the inner divertor plasma will play a much more important role than in the present case. It is therefore very valuable to have the

most basic case successfully 'under our belt'. We can now proceed more confidently to the more challenging cases knowing that we understand – or at least can characterize quantitatively – the problem up to the point of the initial deposition on the inner target.

Conclusions

This study identified and quantified 4 control variables governing the ^{13}C deposition and core contamination behaviour: (a) ~50% conversion efficiency of $^{13}CH_4$ to $^{13}C^+$, (b) $^{13}C^+$ source ~ 3 to 6 cm outboard of the separatrix near the $^{13}CH_4$ injection location, (c) $D_\perp \sim 0.3\ m^2s^{-1}$, (d) $M_{||} \sim 0.4$ toward inside. Modest variations of each of these quantities are also consistent with experiment. There is no evidence, for the plasma conditions involved in the present study, of substantial erosion and re-deposition of the ^{13}C. It thus constitutes the simplest possible case and provides a valuable basis on which to proceed to the general case where redistribution of the initial deposition pattern occurs by ongoing plasma impact.

Acknowledgements

The authors would like to acknowledge the support of a Collaborative Research Opportunities Grant from the Natural Sciences and Engineering Research Council of Canada and the U.S. D.O.E.

References

1. S. Allen, et al, this Conf.
2. W. Wampler, et al, this Conf.
3. A. McLean, et al, this Conf.
4. P.C. Stangeby et al, JNM 313-316 (2003) 883.
5. S. Lisgo, et al, this Conf.
6. J.P. Coad, et al, JNM 290-293 (2001) 224.

Figure Captions

1. Comparison of Langmuir Probe I_{sat} and OSM Input I_{sat}. The I_{sat} is one of the key inputs to the OSM. Ψ_n is the normalized magnetic coordinate.
2. 2a,2b,2c Comparison of the experimental and modeled D_α, D_β and D_γ spectroscopy at Inner target. All figures are scaled in units of photons/m2/s/sr. The modeled hydrogen spectroscopy is produced by EIRENE running with the OSM plasma solution as input. This identified the value of T_e at the inner target as ~ 0.8 ± 0.2 eV.
3. Comparison of upstream n_e and T_e for Thomson (TS), Reciprocating probe (RCP) and the OSM solution. The TS and RCP profiles did not line up exactly, perhaps due to uncertainties in the identifying the separatrix locations, and were slightly shifted (Thomson outward by 0.01 Ψ_n and RCP inward by 0.03 Ψ_n) to match the OSM result. The OSM profiles are essentially based on the target plasma conditions, where the location of the separatrix may be easier to identify, e.g. from the peak in the I_{sat} profile, Fig. 1.
4. Deposition as a function of $M_{||}$ - the parallel flow mach number
5. Deposition as a function of $D_\perp$
6. Deposition as a function of initial $^{13}C^+$ radial position plotted as the distance to the launch position from the separatrix
7. Table – Density of carbon just inside the core plasma for a range of simulation conditions.

Figure 1: Comparison of Langmuir Probe Isat and OEDGE Input Isat

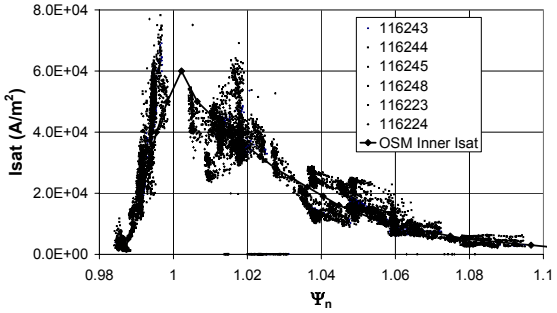

Figure 2: Comparison of modeled and experimental hydrogen emission at the inner target

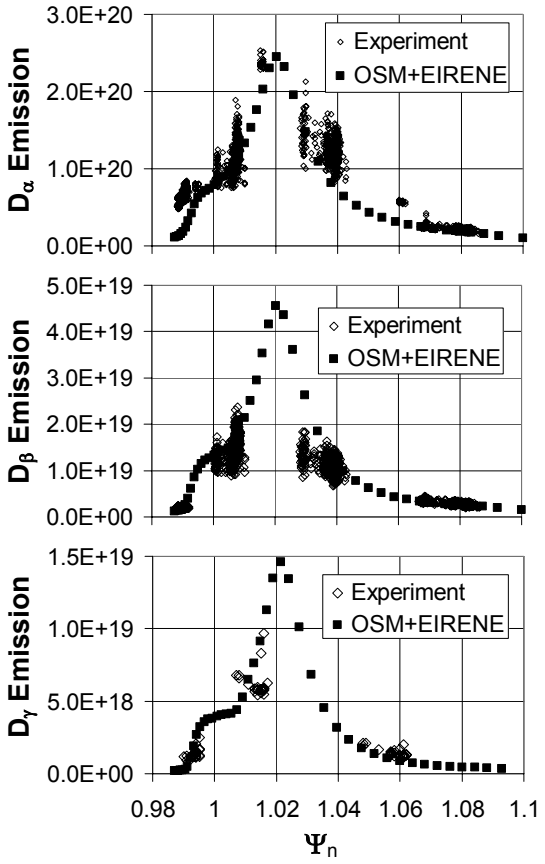

Figure 3: Upstream comparison of OSM, Thomson and RCP for n_e and T_e

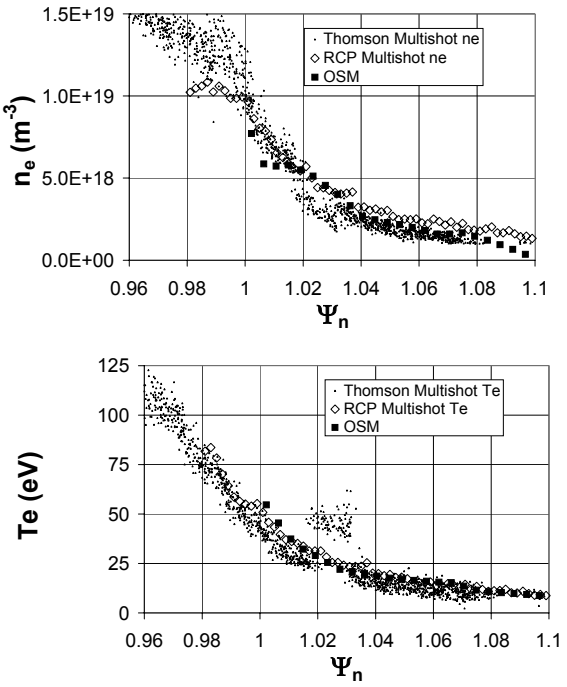

Figure 4: ^{13}C Deposition as a function of the plasma flow mach number

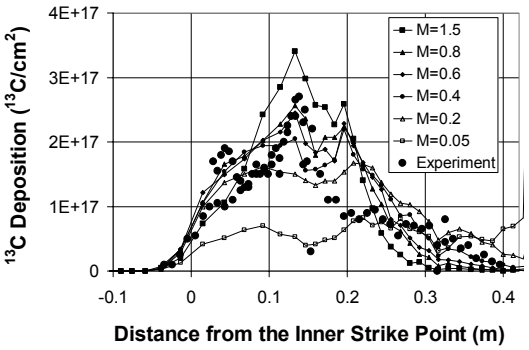

Figure 5: ^{13}C Deposition as a function of $D_{\perp}$

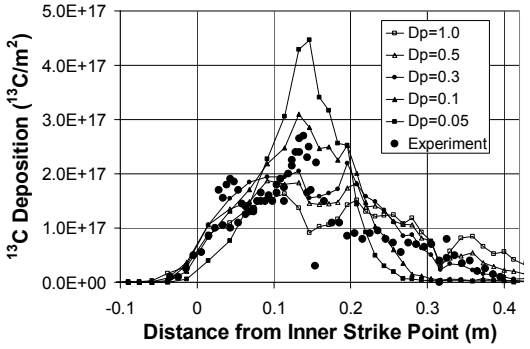

Figure 6: ^{13}C Deposition as a function of the initial ^{13}C radial position

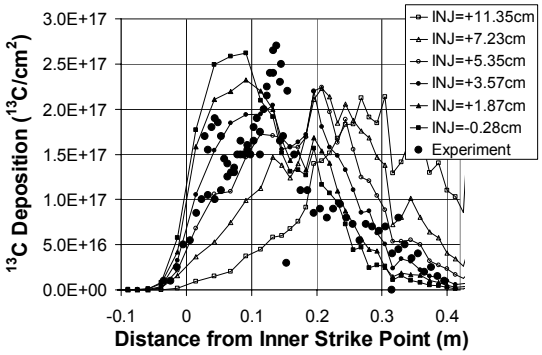

Table 1: ^{13}C Core Edge Density for a range of simulation conditions

Case Mach Number	Core Edge Density (C/m^3)	$D_\perp$	Case	Core Edge Density	Case Distance from Separatrix (cm)	Core Edge Density
M=2.0	1.40E+15		$D_\perp$=1.0	2.59E+16	11.35cm	9.36E+14
M=1.5	2.94E+15		$D_\perp$=0.5	2.58E+16	9.22cm	2.92E+15
M=1.0	6.25E+15		$D_\perp$=0.3	2.61E+16	7.23cm	6.68E+15
M=0.9	8.74E+15		$D_\perp$=0.1	1.40E+16	5.35cm	1.33E+16
M=0.8	9.74E+15		$D_\perp$=0.05	4.50E+15	3.56cm	2.61E+16
M=0.7	1.19E+16				1.87cm	4.40E+16
M=0.6	1.50E+16				0.26cm	7.88E+16
M=0.5	1.93E+16				-0.28cm	9.65E+16
M=0.4	2.61E+16					
M=0.3	3.66E+16					
M=0.2	5.81E+16					
M-0.1	1.14E+17					
M=0.05	2.11E+17					

PSI-16 Paper Length Calculation

The length of the manuscript is computed in terms of the number of single-column journal width lines.

All calculations and/or numbers inside brackets (**[xxx]**) are to be rounded up to the next full integer

Limits: 487 lines (oral/poster); 694 lines (invited/long oral); 795 lines (Review)

We strongly advised you to adhere to these limits. The paper may not be accepted for the refereeing process if too long.

			[round up]
1) Title			
number of characters (including spaces) in title	65	**[x6/58] =**	12
number of characters (including spaces) in author list	220	**[x4/81] =**	12
number of affiliations	6	x2 =	12
Blank lines required by journal added to above			17
Lines in title section			**53**
2) Abstract: A maximum of 150 words is allowed.			
number of words in abstract	148	**[x1/10] =**	15
Blank lines required by journal added to above			18
Lines in abstract section			**33**
3) Body: Account for words in the body text and spaces between sections and sub-sections.			
number of words in body text	1787	**[x1/9] =**	199
number of sections (include acknowledgements)	5	x4 =	20
number of sub-sections	0	x2 =	0
Lines in body			**219**
4) Figures: All figures should be scaled to either 75 (1 column) or 160 mm (2 column) width.			
Total height (in mm) of 75 mm wide figures	376	**[x 0.26] =**	98
number of words in 75 mm wide figure captions	213	**[x1/8] =**	27
number of 75 mm wide figures	6	x2 =	12
Total height (in mm) of 160 mm wide figures	0	**[x 0.52] =**	0
number of words in 160 mm wide figure captions		**[x1/9] =**	0
number of 160 mm wide figures	0	x4 =	0
Lines in figures + captions			**137**
5) Tables			
number of lines (including headings) in 75 mm wide tables	16	x1 =	16
number of words in 75 mm wide table captions	16	**[x1/8] =**	2
number of 75 mm wide tables	1	x3 =	3

number of lines (including headings) in 160 mm wide tables		x2 =	0
number of words in 160 mm wide table captions and footnotes		**[x1/9] =**	0
number of 160 mm wide tables		x6 =	0
Lines in tables + captions			**21**

6) Equations

number of characters in 75 mm wide equations		**[x 1/40] x 3 =**	0
number of 75 mm wide equations		x2 =	0
number of characters in 160 mm wide equations		**[x 1/100] x 6 =**	0
number of 160 mm wide equations		x4 =	0
Lines in equations			**0**

7) References

Lines in references	6	**[x2.16] =**	**13**

8) Journal space for contact information 11

9) Total number of lines from steps 1-8 **487**